Int J Clin Exp Med 2020;13(3):1501-1508
www.ijcem.com /ISSN:1940-5901/IJCEM0106714

*Original Article*

# The distribution of extracranial segments of healthy facial nerves with diffusion tensor imaging: an exploratory study

Yi Qin[1,2], Xuening Zhang[2], Jihua Liu[1], Wentao Liu[1], Peng Li[1], Chunpu Guo[1], Yan Wang[1]

*[1]Medical Imaging Department, The First Affiliated Hospital, Tianjin University of Traditional Chinese Medicine, Tianjin 300193, China; [2]Medical Imaging Department, The Second Hospital of Tianjin Medical University, Tianjin 300211, China*

Received October 31, 2019; Accepted January 5, 2020; Epub March 15, 2020; Published March 30, 2020

**Abstract:** The present study aimed to determine whether an extracranial segment of the facial nerve could be delineated using diffusion tensor imaging (DTI) tractography. A total of 16 volunteers with healthy facial nerves received high-definition 3D-T1WI-1 mm and high-definition DTI scanning in a 3T-MR imaging system. The SPM-old norm method was used in the present study, which enabled the 16 volunteers to have their 3D-T1WI-1 mm to be matched with MNI152_T1_0.5 mm, and establish horizontal T1WI standard templates of 0.5-mm layer thick groups containing parotid glands. The common interest region with a diameter of 10 mm was calculated via fslmaths, and this was placed in the facial nerve stem in the foramen. TrackVis and its Diffusion Toolkit software were used for the facial nerve tracing of the 0.5-mm thin-layer DTI data to obtain the DTI-tractography images of the extracranial segment of facial nerves of the 16 volunteers in the standard space distribution at the group level, and the fractional anisotropy (FA) and mean diffusivity (MD) values of the extracranial segment of the facial nerve. Then, a statistical analysis was conducted. A binary mask was applied for all images to obtain the distribution of the extracranial segments of the facial nerve. However, there was no statistical difference in FA and MD values of the extracranial segment of facial nerves on both sides in healthy subjects. In conclusion, although the facial nerve distribution in the horizontal tracing group level in the present study had a certain error, this basically met the extracranial facial nerve distribution mode of the anatomical study. Large sample facial nerve scanning could perhaps reduce the error, and allow for a more accurate evaluation of the distribution of the extracranial segment of the facial nerve.

**Keywords:** Extra-cranial segment facial nerve, diffusion tensor imaging, parotid gland, anatomy

## Introduction

A number of studies have been conducted on facial nerve dissection of the parotid glands using the T1*- or T2*-weighted volume 3D MR sequences, such as the sequences of 3D-GRASS, 3D-PSIF and 3D-DESSWE, and facial nerves show a high signal or low signal in T1-like or T2-like sequences [1-3]. A traditional 3D MR sequence can display the main branches of the extracranial segment facial nerve trunk, neck surface trunk and temporal surface trunk, but this cannot perform an analysis on the plexus of the intraparotid facial nerve. There are heavier bone and air artifacts around the extracranial segment facial nerve. Hence, there is a certain difficulty in scanning the parotid plexus of facial nerves by conventional thick-slice diffusion tensor imaging (DTI). Previous studies have adopted the 2-mm-layer thick single-shot DTI sequence (single-shot spin-echo DTI sequence) to track facial nerves in the parotid glands, and used super-resolution techniques (MRtrix3 software) to perform the post-treatment of the technique layer 0.3-$mm^3$ of the original DTI sequence to obtain the facial nerve tract DTI nerve fiber tracking images in the parotid glands [4, 5]. Furthermore, the 0.4-$mm^3$ voxel 30-direction DTI sequence was used to scan a one-year-old infant's body specimen, with a data acquisition cost of 15 hours [6], and the fractional anisotropy (FA) map of facial nerves in the temporal bone was obtained using the Brain-Voyager software v20.6 (Brain Innovation,

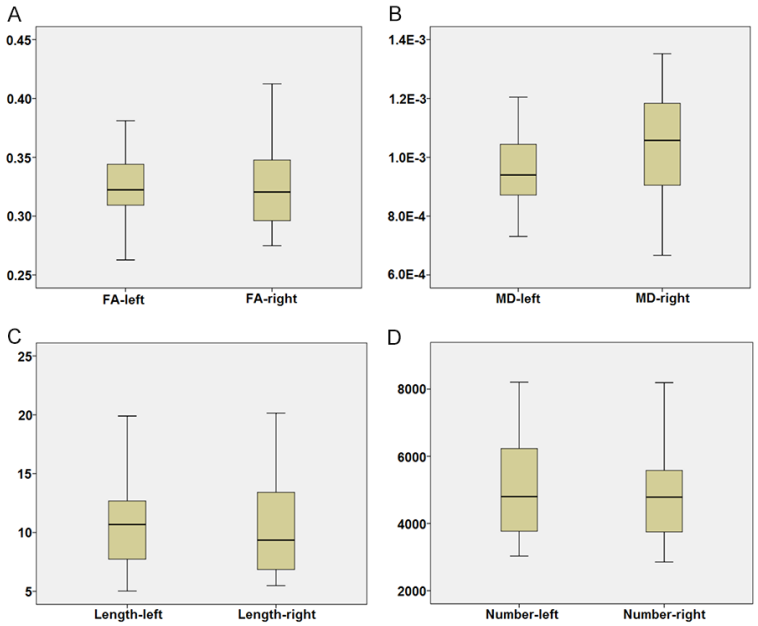


**Figure 1.** Boxplots of the FA (A), MD (B), average length (C) and number of facial nerve fibers (D) for the left and right group. FA: fractional anisotropy; MD: mean diffusivity.

Maastricht, Netherlands). However, DTI nerve fiber tracking was not performed.

Readout-segmented echo-planar diffusion-weighted imaging (RESOLVE) is a kind of multi-shot DTI sequence, which can reduce the influence of bone, air and other magnetic sensitive artifacts on the image. In the present study, 20-direction RESOLVE sequence was used for facial nerve scanning, and the scanned area included facial nerves in the temporal bone and outside the skull. Conventional standard templates, such as the Montreal Neurological Institute (MNI) template, merely contain a small quantity of extracranial anatomical structures, and most of the sectional areas of the extracranial facial nerve are not included. Hence, the facial nerve DTI data cannot be placed in the same standard space. At present, no study has analyzed the extracranial segment of facial nerves at the group level using the DTI sequence.

In the present study, SPM-old norm and FMRIB Software Library (FSL) toolkits were used. Furthermore, affine transformation and nonlinear matching methods were used to place the T1WI images and DTI data of all volunteers in the same standard space, and the data interpolation was up to 0.5 mm layer thick [7, 8]. The 10 mm-diameter spherical region of interest with the same size was located on both sides of the stylomastoid foramen. The group-level analysis was conducted on the FA and mean diffusivity (MD) values of facial nerves on both sides, as well as DTI nerve fiber tracing.

## Materials and methods

### *Subjects*

All 16 volunteers had normal facial nerves, including 15 right-handed and 1 left-handed (10 women and 6 men; mean age: 40.8±6.5 years; range: 23-52 years), who had BMI (body mass indexes) of 19.7-26.9, two of which were rejected for their BMI values above 30.

### *Magnetic resonance (MR) imaging procedures*

A 3.0T MR scanner (MagnetomSkyra; Siemens Healthcare, Erlangen, Germany) with a head-neck phased-array coil and 16 channels was used. The following sequences were performed: sagittal 3D magnetization-prepared rapid acquisition gradient echo (MP-RAGE) sequence with a voxel size 1.0 $mm^3$ (TR = 2,000 ms, TE = 1.97 ms, and FOV = 256 × 256 mm), and axial DTI sequence, which was named, RESOLVE.

The parameters of the RESOLVE sequence were as follows: TR: 4,290 ms, TE1: 71 ms, TE2: 105 ms, diffusion-sensitive factor b = 0 and 1,000 s/$mm^2$, 20 directions, acquired voxel size: 1.2 × 1.2 × 3.0 $mm^3$ with a slice thickness 3 mm, field of view: 220 × 220 mm, multi-shot spin-echo sequence, slices: 30, and scan duration time 12.49 seconds.

### *Data post-processing*

The SPM-old norm method was used for the radiation transformation and nonlinear matching of the 3D-T1-MPRAGE-1 mm image and MNI152_T1_0.5 mm brain template (International Consortium for Brain Mapping) of all volunteers. Furthermore, the bonding box (-90 -126 -108; 90 90 108) created the group-level

**Table 1.** FA and MD values, and numbers of both sides of the facial nerve (mean ± SD)

| | Left | Right | *P* value |
|---|---|---|---|
| FA value | 0.326±0.040 | 0.323±0.036 | 0.700 (t = 0.393) |
| MD value ($10^{-3}$ $mm^2/s$) | 0.970±0.148 | 1.039±0.190 | 0.063 (t = -2.005) |
| Average length of nerve fibers (mm) | 10.784±4.116 | 10.517±4.619 | 0.864 (t = 0.175) |
| Number of nerve fibers | 5073±1633 | 5013±1716 | 0.897 (t = 0.132) |

Note: FA: fractional anisotropy; MD: mean diffusivity.

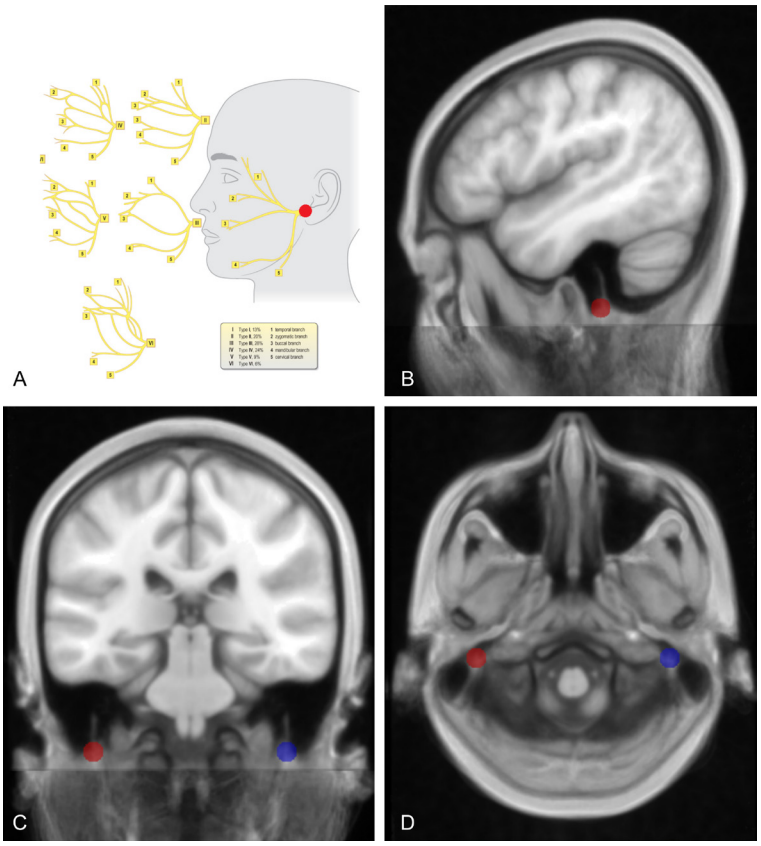


**Figure 2.** The branch of the facial nerve in the parotid gland in format (A) of the anatomy has six distribution forms, with the proportion of the distribution accounting for 6%-28%. There was no absolute dominant type facial nerve distribution, and the area in red presents the diagram of the region of interest. In (B-D), the MNI map with a 0.5-mm layer thickness was overlaid with the average T1WI of the 0.5-mm layer thickness of all volunteers. This is the area of the extracranial segment facial nerve region of interest on two sides of the facial nerve, from the stylomastoid foramen to the entrance of the parotid gland. The regions of interest on two sides were consistent in size and shape, and symmetrical in position. MNI: Montreal Neurological Institute; T1WI: T1 weighted image.

template that contained parotid glands, and the voxel size of T1WI was reduced to 0.5 mm from 1 mm, and was named, the 3D-T1WI-0.5 mm template. Group-level secondary matching was conducted to the image of each volunteer after the norm with the same method. The 3D-T1WI-0.5 mm template from that subject was smoothed using a Gaussian kernel, with FWHM = 8 mm, and this was normalized to the other 3D-T1WI-0.5 mm templates, which included both affine and non-linear matching, with the same enlarged bonding box (-90 -126 -108; 90 90 108) (SPM12-old norm).

Then, FSL (Oxford, UK) was used for the eddy-current correction of DTI data, but brain peeling was not conducted. Then, the DTI data obtained after the eddy-current correction was used for radiation transformation and nonlinear matching with the respective 3D-T1WI-0.5 mm group-level common template of the volunteers. The voxel of the DTI image after matching was reduced to 0.5 mm. The DTI map after matching interpolation was calculated for indexes using the Diffusion Toolkit to obtain the FA map and MD map (mean diffusivity).

Furthermore, fslmath was used for the group-level T1WI-0.5 mm average template to respectively calculate the two 10-mm-diameter spherical regions of interest in the position of stylomastoid foramen facial nerve that went out of the skull on two sides (**Figure 1**). TrackVis and its Diffusion Toolkit software were used for facial nerve tracing, with a FA threshold value of >0.15 and an angle threshold value of 60°.

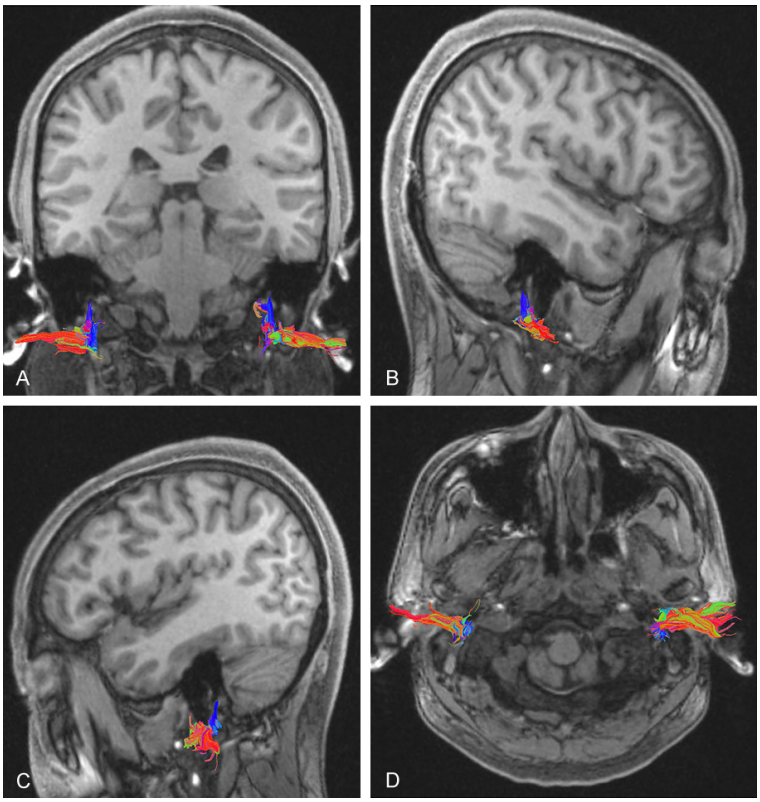


**Figure 3.** The facial nerve DTI tracing of healthy volunteers is shown. A: Coronary; B: Right sagittal position; C: Left sagittal position; D: Bilateral transverse facial nerve distribution. The facial nerve distribution forms on two sides were basically symmetrical. DTI: diffusion tensor imaging.

*Statistical analysis*

For the overall analysis of the facial nerve, descriptive statistics for the qualitative data were developed after pooling the right and left sides, while the quantitative data were averaged across both sides. A normality test was conducted first with a sig of 0.167. This procedure was performed to simplify the presentation of the results. For the quantitative measurements, paired *t*-test was performed to assess the FA and MD value, and the average lengths and numbers of the facial nerve side-to-side differences. All tests for statistical significance were performed for two-tailed hypotheses, with $P<0.05$. The statistical calculations were performed using the Statistical Package for the Social Sciences, Version 18 (SPSS, Chicago, Illinois, USA).

## Results

All FA and MD maps were successfully obtained from the 16 healthy volunteers. No statistical difference was obtained for FA, MD and numbers in both sides of the facial nerve ($P>0.05$, **Table 1** and **Figure 1**). The facial nerve distribution that formed on both sides was basically symmetrical.

The red circular region in **Figure 2A** presents a diagram of the region of interest with a diameter of 10 mm, and the two sides were consistent in size and shape, and symmetrical in position. The volume was calculated using fslmath from the coronal, sagittal and axial planes (**Figure 2B-D**). The facial nerve DTI tracing of one healthy volunteer is presented in **Figure 3**. If the facial nerve distribution was regarded to exceed 6% of the lowest distribution probability, this would be deemed as a facial nerve in the parotid gland, as shown in **Figure 4A-D** (red and blue). If the facial nerve distribution was regarded to exceed 50% of the lowest distribution probability, this would be deemed as the facial nerve trunk, as shown in **Figure 2A-D** (green and pink). If half of the average probability of 16.7% is exceeded, this indicates that the maximum distribution probability of the facial nerve is in the parotid gland, as shown in **Figure 5A-D**.

## Discussion

In parotidectomy, iatrogenic injury of the facial nerve should be avoided, and the protection of the facial nerve remains as a key problem during surgery [9-12]. The extracranial segment of the facial nerve enters into the parotid gland from the stylomastoid foramen, and this can be divided into the temporofacial branch and cervicofacial branch, two trunks, and five branches. Davis *et al.* dissected 350 cervicofacial halves, and discovered that the parotid gland segment facial nerve branch is distributed in six forms, and the distribution of each form was not in the leading dominant position, with the maximum distribution form accounting for 28%, the minimum distribution form accounting for

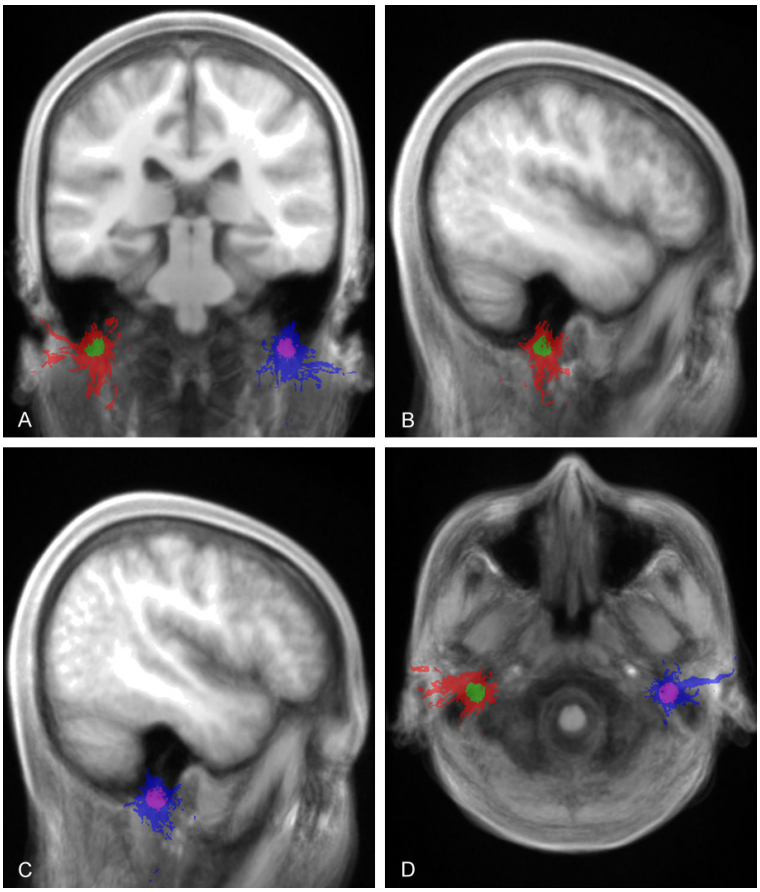


**Figure 4.** The bilateral facial nerve group level distribution map is shown (threshold value of 6%): left (red) and right (blue); the bilateral main trunks of the facial nerve (>50%): left (green) and right (pink). A: Coronary position; B: Right sagittal position; C: Left sagittal position; and D: Transverse position.

6%, and the remaining distribution forms accounting for 9%, 13%, 20% and 24%, respectively; and the average distribution probability is 16.7% [13, 14]. In another study conducted by Ellis et al., 46 corpses and 22 skulls were dissected, and the following were discovered: except for the fixed position of the facial nerve trunk from the stylomastoid foramen to the tympanomastoid fissure end towards 10 mm inwards, other facial distal distribution forms were very complicated, and even one person's bilateral facial nerve distribution was inconsistent [15]. In the present study, in the area where the bilateral stylomastoid foramen went out of the skull in the group level T1WI template, fslmath was used to calculate the spherical common region of interest, and DTI nerve fiber tracing was performed for the bilateral extracranial facial nerves. Although norm treatment was conducted for each volunteer's T1WI in the present study, each volunteer's subcutaneous fat thickness differed, and the position of stylomastoid foramen still probably had some differences. Therefore, a bigger the spherical region of interest of 10 mm in diameter was adopted for the present study [16].

Due to the uncertainty of the extracranial segment facial nerve, and in combination with the anatomy results of previous studies [9-12], if the volunteers in the group had a voxel coexistence of more than 6%, this would be regarded as facial nerve existence, as shown in **Figure 4** (right: red, left: blue), indicating that the facial nerve network in the parotid gland could be identified. However, if the volunteers in the group had a voxel coexistence of more than 50%, this would be regarded as facial nerve trunk existence, as shown in **Figure 4** (right: green, left: pink), indicating the fixing of facial nerve trunk position. Furthermore, if the average probability was exceeded (one half of 16.7, i.e. 8.35% was the maximum distribution probability of the facial nerve; **Figure 5**), this indicates the starting points of the temporofacial trunk, cervicofacial trunk and cheek branch of the facial nerve. The facial nerve constitutes a complicated nerve plexus in the parotid gland (**Figure 4**), and this shows that no expected facial nerve injury was caused after the tiny branch of the facial nerve in the parotid gland was damaged.

Since the extracranial segment facial nerve was located in the subcutaneous superficial position and close to the skull base, and there were external carotid arteries and veins, and lymph vessel running in the parotid gland, more magnetic sensitive artifacts and flow artifacts may be caused to influence the display of the facial nerve. The RESOLVE DTI sequence adopted for the present study differed from the traditional DWI single-shot one-time filling of all k

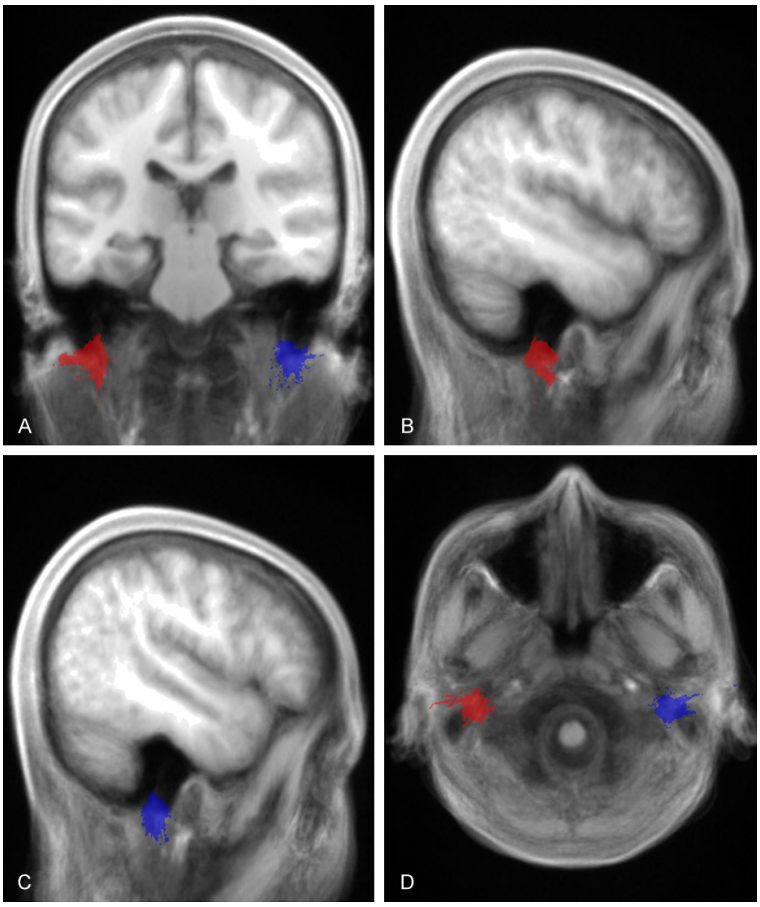


**Figure 5.** The average distribution probability of more than six variations of bilateral facial nerves is 16.7%, which exceed the average distribution probability of 50%. That is, the distribution probability map of 8.35%, which was named the maximum probability map of the intraparotid facial nerve: left (red) and right (blue). A: Coronary; B: Bight sagittal position; C: Left sagittal position; and D: Transverse position.

space data. RESOLVE adopted the multi-shot and block-read-out acquisition method, and real-time motion correction was used to significantly reduce and even eliminate the magnetic sensitive artifacts and blurring effect. The obtained FA and MD values were stable with high repeatability [17-19].

In the present study, the RESOLVE data of all volunteers was subjected to affine and non-linear terms. Furthermore, all the RESOLVE data was standardized into the same space by virtue of the MNI-152-0.5 mm and personal T1WI-0.5 mm template after norm. In addition, the voxel of RESOLVE was reduced to 0.5 $mm^3$. Since the volunteers had different subcutaneous fat thicknesses, and the anatomical structures of the parotid gland, mastoid and belonoid around the extracranial segment facial nerve had more variations, these were difficult to be removed, which is similar to the cerebrospinal fluid around the spinal cord [20]. In the present study, no arbitrary volunteer was selected as a standard space template, but each volunteer's own DTI data and his/her own T1WI map after old-norm were matched to the same space to avoid data distortion after matching [21]. The FA value, MD value, and number of nerve bundle fibers of the bilateral extracranial segment facial nerve in the present study had no statistical differences.

The limitation of this study was that despite the control of the BMI index and after the SPM-old norm, each volunteer's T1WI map was basically in the same space (**Figure 2**). Furthermore, the volunteers still had some differences in subcutaneous fat thickness, parotid gland, mastoid and belonoid forms, and there was no recognized standard template that contains the extracranial segment facial nerve at present, similar to the brain MNI template, such as the MNI template. Hence, the extracranial segment facial nerve cannot fully realize the point-to-point matching. Therefore, it was held that there would be a certain error when the extracranial segment facial nerve distribution at the group-level was calculated. In addition, although the RESOLVE sequence can improve the SNR of the DTI image, it a had longer scanning time than the traditional single-shot DTI sequence. Furthermore, the RESOLVE scanning range in the present study contained the cerebellum and temporal bone, which contained the facial nerve in the temporal bone, thereby realizing a better matching by virtue of the brain mass and structure image. Therefore, although the interlayer voxel of the RESOLVE scanning was 1.2 × 1.2 mm in size, the interlayer thickness was 3 mm, and the

reduction of the interlayer thickness would cause a longer RESOLVE scanning time.

In conclusion, although the facial nerve distribution of the horizontal tracing group level in the present study had a certain error, this basically met the extracranial facial nerve distribution mode of the anatomical study. Large sample facial nerve scanning could perhaps reduce the error, and allow for more accurate evaluation of the extracranial segment of facial nerve distribution.

## Acknowledgements

We would like to thank Dr. Wen Qin from Tianjin Medical University General Hospital for his kind help regarding the data analysis after DTI.

## Disclosure of conflict of interest

None.

**Address correspondence to:** Xuening Zhang, Medical Imaging Department, The Second Hospital of Tianjin Medical University, No. 23, Pinjiang Road, Hexi District, Tianjin 300211, China. Tel: +86-22-88329422; Fax: +86-22-27986079; E-mail: Luckyxn@126.com

## References

[1] Qin Y, Zhang J, Li P and Wang Y. 3D double-echo steady-state with water excitation MR imaging of the intraparotid facial nerve at 1.5T: a pilot study. AJNR Am J Neuroradiol 2011; 32: 1167-1172.

[2] Radhakrishnan R, Ahmed S, Tilden JC and Morales H. Comparison of normal facial nerve enhancement at 3T MRI using gadobutrol and gadopentetate dimeglumine. Neuroradiol J 2017; 30: 554-560.

[3] Guenette JP, Seethamraju RT, Jayender J, Corrales CE and Lee TC. MR imaging of the facial nerve through the temporal bone at 3T with a noncontrast ultrashort echo time sequence. AJNR Am J Neuroradiol 2018; 39: 1903-1906.

[4] Attyé A, Karkas A, Troprès I, Roustit M, Kastler A, Bettega G, Lamalle L, Renard F, Righini C and Krainik A. Parotid gland tumours: MR tractography to assess contact with the facial nerve. Eur Radiol 2016; 26: 2233-2241.

[5] Rouchy RC, Attyé A, Medici M, Renard F, Kastler A, Grand S, Tropres I, Righini CA and Krainik A. Facial nerve tractography: a new tool for the detection of perineural spread in parotid cancers. Eur Radiol 2018; 28: 3861-3871.

[6] Ginat DT, Collins J, Christov F, Nelson EG and Gluth MB. Delineation of the intratemporal facial nerve in a cadaveric specimen on diffusion tensor imaging using a 9.4T magnetic resonance imaging scanner: a technical note. Radiol Phys Technol 2019; 12: 357-361.

[7] Guntinas-Lichius O, Silver CE, Thielker J, Bernal-Sprekelsen M, Bradford CR, De Bree R, Kowalski LP, Olsen KD, Quer M and Rinaldo A. Management of the facial nerve in parotid cancer: preservation or resection and reconstruction. Eur Arch Otorhinolaryngol 2018; 275: 2615-2626.

[8] Savvas E, Hillmann S, Weiss D, Koopmann M, Rudack C and Alberty J. Association between facial nerve monitoring with postoperative facial paralysis in parotidectomy. JAMA Otolaryngol Head Neck Surg 2016; 142: 828-833.

[9] Wilke M, Altaye M, Holland SK and Consortium CA. CerebroMatic: a versatile toolbox for spline-based MRI template creation. Front Comput Neurosci 2017; 11: 5.

[10] Richards JE, Sanchez C, Phillips-Meek M and Xie W. A database of age-appropriate average MRI templates. Neuroimage 2016; 124: 1254-1259.

[11] Bly RA, Holdefer RN, Slimp J, Kinney GA, Martinez V, Manning SC and Perkins JA. Preoperative facial nerve mapping to plan and guide pediatric facial vascular anomaly resection. JAMA Otolaryngol Head Neck Surg 2018; 144: 418-426.

[12] Ansó J, Dür C, Apelt M, Venail F, Scheidegger O, Seidel K, Rohrbach H, Forterre F, Dettmer MS and Zlobec I. Prospective validation of facial nerve monitoring to prevent nerve damage during robotic drilling. Front Surg 2019; 6: 58.

[13] Davis RA. Surgical anatomy of the facial nerve and parotid gland based upon a study of 350 cervicofacial halves. Surg Gynecol Obstetr 1956; 102: 385-412.

[14] Hirsch BE. Gray's anatomy: the anatomical basis of clinical practice. JAMA 2009; 301: 1825-1831.

[15] Ellis GS. Akinesia of the facial nerve: a laboratory investigation of the surgical anatomy. Trans Am Ophthalmol Soc 1968; 66: 746.

[16] Karaca H, Soydan L, Yildiz S and Toros SZ. Measurement of the depth of facial nerve at the level of stylomastoid foramen using MR imaging in Bell's palsy. Clin Imaging 2019; 58: 34-38.

[17] Liney GP, Holloway L, Al Harthi T, Sidhom M, Moses D, Juresic E, Rai R and Manton DJ. Quantitative evaluation of diffusion-weighted imaging techniques for the purposes of radiotherapy planning in the prostate. Br J Radiol 2015; 88: 20150034.

[18] Friedli I, Crowe LA, Viallon M, Porter DA, Martin PY, de Seigneux S and Vallée JP. Improvement

of renal diffusion-weighted magnetic resonance imaging with readout-segmented echo-planar imaging at 3T. Magn Reson Imaging 2015; 33: 701-708.

[19] Tokoro H, Fujinaga Y, Ohya A, Ueda K, Shiobara A, Kitou Y, Ueda H and Kadoya M. Usefulness of free-breathing readout-segmented echo-planar imaging (RESOLVE) for detection of malignant liver tumors: comparison with single-shot echo-planar imaging (SS-EPI). Eur J Radiol 2014; 83: 1728-1733.

[20] Eippert F, Finsterbusch J, Bingel U and Büchel C. Direct evidence for spinal cord involvement in placebo analgesia. Science 2009; 326: 404.

[21] Peng H, Orlichenko A, Dawe RJ, Agam G, Zhang S and Arfanakis K. Development of a human brain diffusion tensor template. Neuroimage 2009; 46: 967-980.